

# Integrated system for SHM and wear estimation of railway infrastructures

Nicola Roveri<sup>1</sup>, Antonio Carcaterra<sup>1</sup>, Aldo Sestieri<sup>1</sup>

<sup>1</sup>Department of Mechanics and Aeronautics, University of Rome, 'La Sapienza'  
Via Eudossiana, 18, 00184, Rome, Italy  
{nicola.roveri@gmail.com, carcaterra.antonio@gmail.com, aldo.sestieri@uniroma1.it}

## Abstract

In this work we present the results of a field trial with a FBG sensor array system for the real time monitoring of railway traffic and for the structural health monitoring of both the railway track and train wheels. The test campaigns are performed on the on the 2nd line of Milan metropolitan underground, employing more than 50 FBG sensors along 1,5 km of the rail track, where the trains are tested during daily passenger rail transport, with maximum speeds roughly of 90 km/h. The measurements were continuatively performed for over six months, with a sampling frequency of about 400 Hz. The large amount of data/sensors allow a rather accurate statistical treatment of the measurement data and permit, with dedicated algorithms, the estimation of rail and wheel wear, key traffic parameters such as the number of axles, the train speed and load, and, in the next future, the detection of localised imperfections.

## 1 Introduction

The use of vibration measurements for structural health monitoring has attracted significant research attention during the last three decades [1, 2]. However, the majority of maintaining operations still relies on the direct inspection by experienced workers, such as in the railroad transportation industry. Considering that rail transport has become one of the most employed means of transportation, efficient monitoring devices are crucial to reduce maintenance costs and improve the safety of passengers and goods.

On this ground, strain gauge sensors are generally adopted to monitor key parameters, such as axle load, train speed and wheel defects. Even if the technology is well consolidated, it is not very efficient for railways, since it is affected by electromagnetic interference [3] and the sensors cannot be easily multiplexed in a single electric cable. More sophisticated techniques, based on ultrasonic [4] and acoustic [5] sensors, have also been employed. However, the accuracy of these sensors is deeply affected by electromagnetic interference from the railroad environment. In the last years, the use of Fiber Bragg Grating technology has become more and more frequent [3, 6, 7], because it overcomes the mentioned problem, assuring immunity to electromagnetic fields and simple multiplexing, fitting a larger number of sensors accompanied with high performance acquisition units. Nevertheless, the complete dynamic characterization of a railway infrastructure is still far from being on the shelf [8, 9].

In this work, we propose in service real-time monitoring of the working conditions of both the rail track and the wheels of the trains, using FBG sensors. The experimental setup is installed along the line two of the subway of Milan, close to the Famagosta station, which is a heavily used suburban railway line with trains running under 90 km/h speeds. The sensors measure the rail strain response under wheel-rail interaction. Given the high number of installed sensors, with a permanent acquisition system, a dedicated statistical algorithm permits to isolate the single contributions of the rail and the wheels from the acquired vibration signal, then to identify their health status.

## 2 Experimental setup

A FBG sensor is a distributed Bragg reflector, i.e. a periodical variation of refractive index, inside the core of optical fiber, able to reflect a particular wavelength of light and transmit all the others. The reflected Bragg wavelength  $\lambda_B$  is related to the refractive index of the fibre  $n$  and to the period of the refractive index modulation  $\Lambda$  by the formula:  $\lambda_B=2n\Lambda$ . Mechanical and thermal perturbations modify the index modulation  $\Lambda$  and the refractive index  $n$  then  $\lambda_B$ . These perturbations can be determined by monitoring the wavelength change of the FBG sensor. Characteristic wavelength variations of FBG sensor, with a central wavelength of 1550 nm, due to mechanical strain and temperature change are roughly  $1\text{pm}/\mu\epsilon$  and  $10\text{ pm}/^\circ\text{C}$ . FBG sensors allow distributed sensing over significant areas by multiplexing a large number of sensors on a single fibre, they are immune to electromagnetic interference and have compact size. For these reasons they have been widely applied in many applications for the structural health monitoring [n14].

In this work, we analyse the data acquired by an experimental set-up consisting of four lines of FBG sensors, installed along a track of the line two of the subway of Milan, close to the Famagosta station. Each line is made of 15 FBG sensors, most of them are placed near the sleeper and work in pure flexion to detect the strain deformation of the rail. Two or three sensors per line are placed near the neutral axis of the rail, as in Fig. 1, and detect the environmental temperature; the spacing between two consecutive sensors is within the range 10-20 m, the whole optical fibres apparatus covers about 1, 2 km of a line track.



Figure 1: FBG sensor installed on the rail neutral line to detect the temperature change.

The FBG sensors were installed during the usual maintenance period, from 1:00 to 4:00, when the regular transportation service is stopped, pasting them directly on the rail track with epoxy resin. Unfortunately, the sensors were not placed by the authors, which had only the chance of analysing the acquired data. As a further improvement, the track will be equipped with an additional optical line with several pair of sensors with a  $45^\circ$  angle of inclination with respect to the rail neutral line and allowing an easy identification of the axle weight [10, 11]. We selected 21 strain sensors among all of them, which present the highest signal to noise ratio, to analyse the recorded data.

The traffic conditions allow recording approximately 80 train passages per day, whose speeds are ranging between 50 and 80 km/h. The train type is MNG M1 “Meneghino” shown in Fig. 2 whose data sheet is given in table I. The rail used is the S 50 UNI type, *Vignole*, the distance between sleepers axis is 0,6 m.

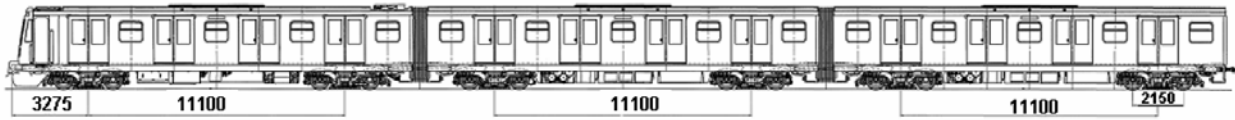


Figure 2: Train type MNG M1 “Meneghino”.

Product class	Treno metropolitano Metro
Customer	ATM Milano
Vehicle type	car body over two bogies
Track gauge	1435 mm
Main traction system	1500 V cc from pantograph - 750 V cc from third track
Total nominal rating power	1280 kW
Coach width	2850 mm
Intermediate coach length	17,57 m
Cab coach length	17,61 m
Maximum speed	90 km/h
Bogie pivot pitch	11,1 m
Bogie pitch motor bogie	2150 mm
Bogie pitch trailer bogie	2150 mm
Wheel diameter	820 mm
Train set mass (tare)	31.7 t
Train set total mass	48.9 t

Table I: Train data sheet.

A schematic description of the measurement chain is shown in Fig. 3:

- a light beam signal, in the range of far infrared wavelengths, is generated by an optical led source; the light beam travels along an optical fiber equipped with FBG sensors attached to the rail;
- when the rail is deformed, the frequency bandwidth of the reflected light changes and such variation is detected by a spectrum analyser;
- the spectrum analyser samples the analogical signal before sending it to the computer and the signal can be suitably processed;
- regarding the FBG interrogator, it was used a prototype model, equipped with four measurement channel, with a wavelength measuring range of 75 nm and a maximum sampling rate of 400 Hz per sensor per channel. The available sampling rate is not very high, however it is adequate to the usual speeds of the trains here analysed, below 90 km/h: the distance between sleepers is indeed covered in about 25 ms;
- each optical line is linked to the interrogator with 2 km of cable. The FBG interrogator and other devices are placed in the maintenance office of the Famagosta train station, 500 m far from the field test.

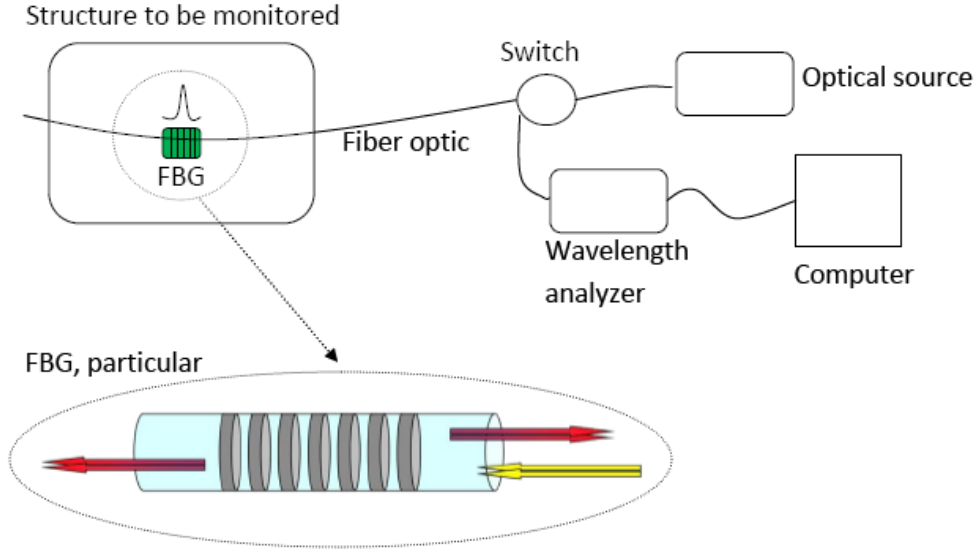


Figure 3: Example of the measurement chain.

### 3 Theoretical formulation of the problem

#### 3.1 Dynamic equation

The information used for the identification process comes from the dynamic equation of the rail. This allows understanding better the rail excitation phenomena and the main spectral characteristics of the acquired signal. The rail can be modelled as a prototype structure consisting of an infinite beam on an elastic foundation carrying a lumped travelling mass due to the inertia of the train mass fraction considered integral to the wheels. This structure is excited by (i) the travelling load of the train mass, (ii) the vertical inertial loads due to the wheel-train mass excited by the rail-wheels geometrical irregularities. Setting  $\rho A$ ,  $EI$ ,  $w(x, t)$ ,  $g$ ,  $\delta(x)$ ,  $x_p(t) = Vt$  and  $v(t)$  the mass per unit length, the flexural stiffness, the displacement of the rail, the standard gravity constant, the Dirac delta function, the time history of the moving load while crossing the bridge and the vertical displacement of the moving mass, respectively, the system is described by:

$$EI \frac{\partial^4 w(x, t)}{\partial x^4} + [\rho A + m \delta(x - Vt)] \frac{\partial^2 w(x, t)}{\partial t^2} + \chi w(x, t) = mg \delta(x - Vt) + m a_w(t) \delta(x - Vt)$$

where the last term on the rhs accounts for the vertical acceleration  $a_w(t)$  of the train mass  $m$  due to the combined random irregularities at a single wheel-rail contact, i.e. a single wheel of the wagon. Therefore:

$$a_w(t) = \frac{d^2}{dt^2} [r(t) + h(t)] = \frac{d^2}{dt^2} [r(\theta)|_{\theta=\Omega t} + h(x)|_{x=Vt}]$$

where  $r(\theta)$  and  $h(x)$  are two random signals. More precisely, the first is related to the wheel geometrical imperfections that make  $r(\theta)$  periodic-random. The randomness is caused by the set of train wheels (of a wagon) that excites the rail, and each of the wheel signals can be considered as a sample of the same random process. The period is controlled by the wheel angular speed  $\Omega$  and wheel radius  $R$ . The signal  $h(x)$  is indeed simply random.

#### 3.2 Rail response spectrum excited by the rail-wheel roughness

The form of the equation of motion suggests two different types of rail responses: the first is related to the load  $mg \delta(x - Vt)$  for which the response can be found in the form  $\Phi_{mg}(x - Vt) = \Phi_{mg}(\xi)$ . Therefore, substituting into the equation of motion one obtains:

$$EI \Phi_{mg}^{iv}(\xi) + \rho AV^2 \left[ 1 + \frac{m}{\rho A} \delta(\xi) \right] \Phi_{mg}''(\xi) + \chi \Phi_{mg}(\xi) = mg \delta(\xi)$$

This equation can be analytically solved considering two solutions: one for positive  $\xi$ , the second for negative  $\xi$  and imposing for the two solutions congruence conditions at  $\xi=0$ . For the purpose of this analysis, we are only interested here to the frequency content of the signals acquired by the sensors. This analysis can be carried out only employing the dispersion relationship associated to the free propagation problem. To this aim, the congruence conditions at  $\xi=0$  is skipped, and the dispersion relationship is found looking for solution of the form  $e^{k\xi}$ :

$$EI k^4 + \rho AV^2 k^2 + \chi = 0 \tag{1}$$

Using general parameters found in the literature for underground railways (MKS units:  $EI=3.7 \cdot 10^6$ ,  $\rho A=50$ ,  $\chi=5 \cdot 10^7$ ), this equation can be solved in terms of  $k$  for different values of the train speed  $V$ , generally  $k = k_r + jk_i$ . This implies the solution is controlled by the factor  $e^{jk_i V t}$  characterized by a circular frequency  $\omega = k_i V$ : the final result for different train speeds is shown in Fig. 4, where the frequency is 2.1Hz for  $V=10$ m/s, 4.3 Hz for  $V=20$  m/s, 10.9 Hz for  $V=50$ m/s.

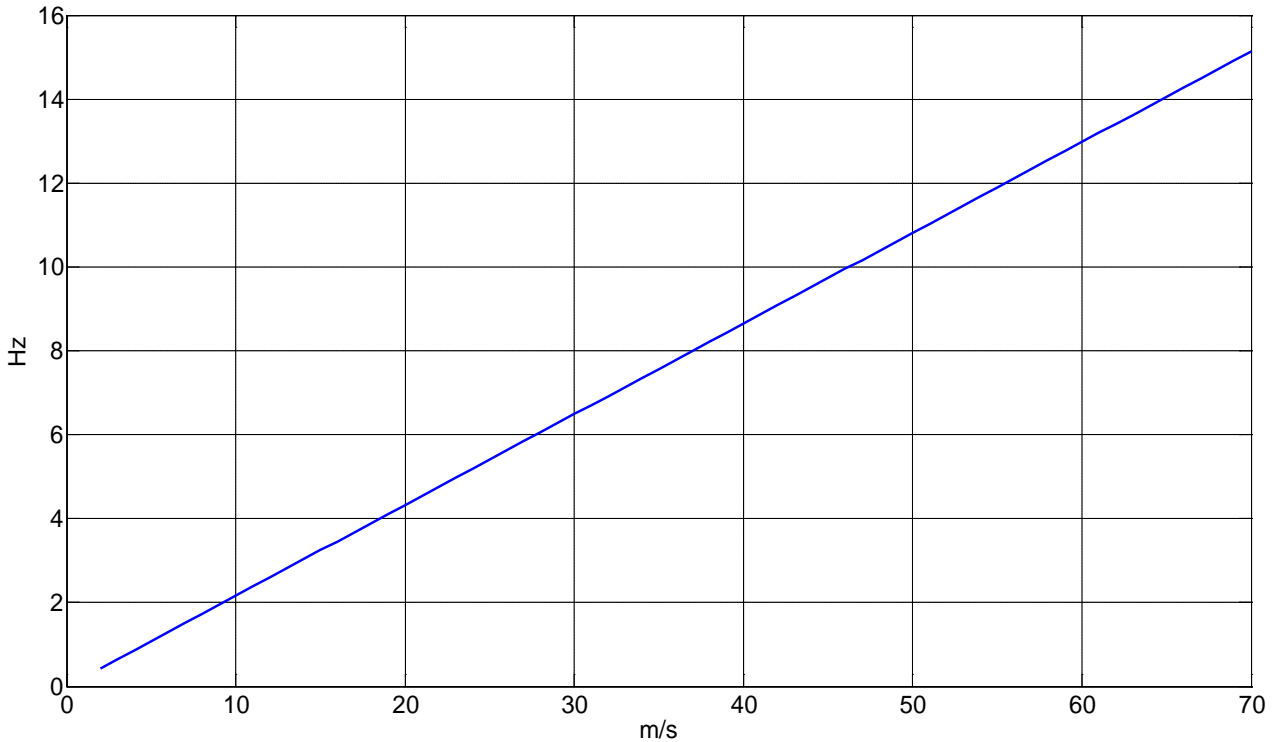


Figure 4: Circular frequency from eq. (1) plotted versus the train speed

The second part of the excitation is trickier. In fact, simple travelling solutions are not admitted, because the wheel excitation is of the form  $ma_w(t)\delta(x - Vt)$ , that contains the product of a traveling term and a time-

dependent function. However, as a general consideration that will be detailed later, the term  $a_w(t)$  can be reduced to a suitable superposition of time-harmonic functions as  $\sum_{n=1}^N C_n e^{j\omega_n t}$  and therefore:

$$m a_w(t) \delta(x-Vt) = m \delta(x-Vt) \sum_{n=1}^N C_n e^{j\omega_n t}$$

This expression allows looking for solutions of the form:

$$w(x,t) = \sum_{n=1}^N C_n \Phi_{ma_w}^n(x-Vt) e^{j\omega_n t} = \sum_{n=1}^N C_n \Phi_{ma_w}^n(\xi) e^{j\omega_n t}$$

where the rail response to the random loads comes from the product of two different factors. The frequency content response of the first  $\Phi_{ma_w}^n(x-Vt)$  can be evaluated using the dispersion relationship, while the second can be derived directly inspecting the harmonic components  $\omega_n$ .

Substituting a single component  $\Phi_{ma_w}^n(\xi) e^{j\omega_n t}$  into the equation of motion, after some mathematics, we have:

$$EI \Phi_{ma_w}^{iv}(\xi) + \rho A [V^2 \Phi_{ma_w}''(\xi) - 2j\omega_n V \Phi_{ma_w}'(\xi) - \omega_n^2 \Phi_{ma_w}(\xi)] + \chi \Phi_{ma_w}(\xi) = 0$$

where the index  $n$  in the  $\Phi$ 's is omitted for sake of notation. Again, the point  $\xi=0$  is skipped, and the dispersion relationship is found looking for solution of the form  $e^{jk\xi}$ :

$$EI k^4 - \rho A k^2 V^2 + 2 \rho A \omega_n k V + \chi - \rho A \omega_n^2 = 0 \quad (2)$$

where the subscript  $k_i$  is omitted. This equation must be solved in terms of  $k$ , varying both the train speed and the harmonic content of the signal (wheel and rail) here represented by  $\omega_n$ .

Before proceeding further, we must distinguish the rail and wheel signal components. For the wheel signal, being it periodic, we use a direct Fourier series representation:

$$r(g) = \sum_{n=1}^N C_n^{(wheel)} e^{jn g} \Rightarrow r(t) = \sum_{n=1}^N C_n^{(wheel)} e^{jn \Omega t}$$

where  $C_n^{(wheel)}$  are coefficients randomly varying when different wheels are considered and  $n\Omega = \omega_n$ , where  $\Omega$ , the wheels angular speed, is to be used in the dispersion relationship. Namely, the minimum circular frequency is trivially equal to  $\omega_{\min} = \omega_1 = \Omega$ . The maximum frequency is simply determined considering that

$$N \approx \frac{\omega_{\max}}{\Omega} = \frac{2\pi}{\Omega \lambda_{\min}} V, \text{ where } \lambda_{\min} \text{ can be found in the literature of technical data about the wheel roughness,}$$

and  $\lambda_{\min} \approx 0.02m$ . This value is associated to the maximum wavenumber in the wheel roughness spectra.

Therefore, using the determined values  $\omega_1, \dots, \omega_N$ , and for a given  $V$  in the dispersion relationship, we can determine the corresponding range  $[k_{\min}, k_{\max}]$  for  $k$  and finally the characteristic frequency range  $[k_{\min} V, k_{\max} V]$  of the factor  $\Phi_{ma_w}^n(x-Vt)$ . The frequency bandwidth of the second factor  $e^{j\omega_n t}$  is indeed

simply  $[\omega_{\min}, \omega_{\max}]$ , where  $\omega_{\max}^{(wheel)} = \omega_{\max}$ . Therefore, the spectrum of the  $\sum_{n=1}^N C_n^{(wheel)} \Phi_{ma_w}^n(x-Vt) e^{j\omega_n t}$

, lies within the range  $[k_{\min}^{(wheel)} V, \omega_{\max}^{(wheel)} + k_{\max}^{(wheel)} V]$ , as it follows by spectral properties of the product of time functions. It is important to remark that  $k_{\min}^{(wheel)}$ ,  $k_{\max}^{(wheel)}$  depend on  $V$  and on  $\omega_{\min}^{(wheel)}$ ,  $\omega_{\max}^{(wheel)}$  as well.

For the rail, we have to use a continuous spectral representation. It can be derived considering a finite length  $L$  of the rail:

$$h(x) = \sum_{n=1}^N C_n^{(rail)} e^{j \frac{2\pi n}{L} x} \Rightarrow h(t) = \sum_{n=1}^N C_n^{(rail)} e^{jn \frac{2\pi V}{L} t}$$

that would produce a periodic representation of the signal over  $L$ . Again, the coefficients  $C_n^{(rail)}$  are random, and  $2\pi nV/L = \omega_n$  would be used in the dispersion equation. However, in the present case, the rail length  $L$  is infinite, and this makes the frequency spectrum continuous and, as it usual in random vibrations, the coefficients  $C_n^{(rail)}$  form the basis for defining the power spectral density of the rail irregularities. Namely, the minimum and maximum circular frequencies to use into the dispersion relationship are determined considering

that  $\omega_{\min} = \frac{2\pi}{\lambda_{\max}} V$ ,  $\omega_{\max} = \frac{2\pi}{\lambda_{\min}} V$ , where both  $\lambda_{\min}, \lambda_{\max}$  can be found in the literature of technical data and

$\lambda_{\min} \approx 0.2m, \lambda_{\max} \approx 20m$ . Therefore, we can proceed as in the previous case to determine frequency bandwidth of the product of the two factors appearing in the rail response. Namely, the spectrum of  $\sum_{n=1}^N C_n^{(rail)} \Phi_{m d_w}^{n(rail)}(x-Vt) e^{j\omega_n t}$  lies within the range  $[k_{\min}^{(rail)} V, \omega_{\max}^{(rail)} + k_{\max}^{(rail)} V]$ .

The conclusion is that the three frequency bandwidths related to the loads  $mg \delta(x-Vt)$ ,  $m\ddot{r}(t) \delta(x-Vt)$ ,  $m\dot{h}(t) \delta(x-Vt)$  are represented in fig 5 and table II. For the three values of the speed  $V$  the bandwidth are calculated following the described procedures.

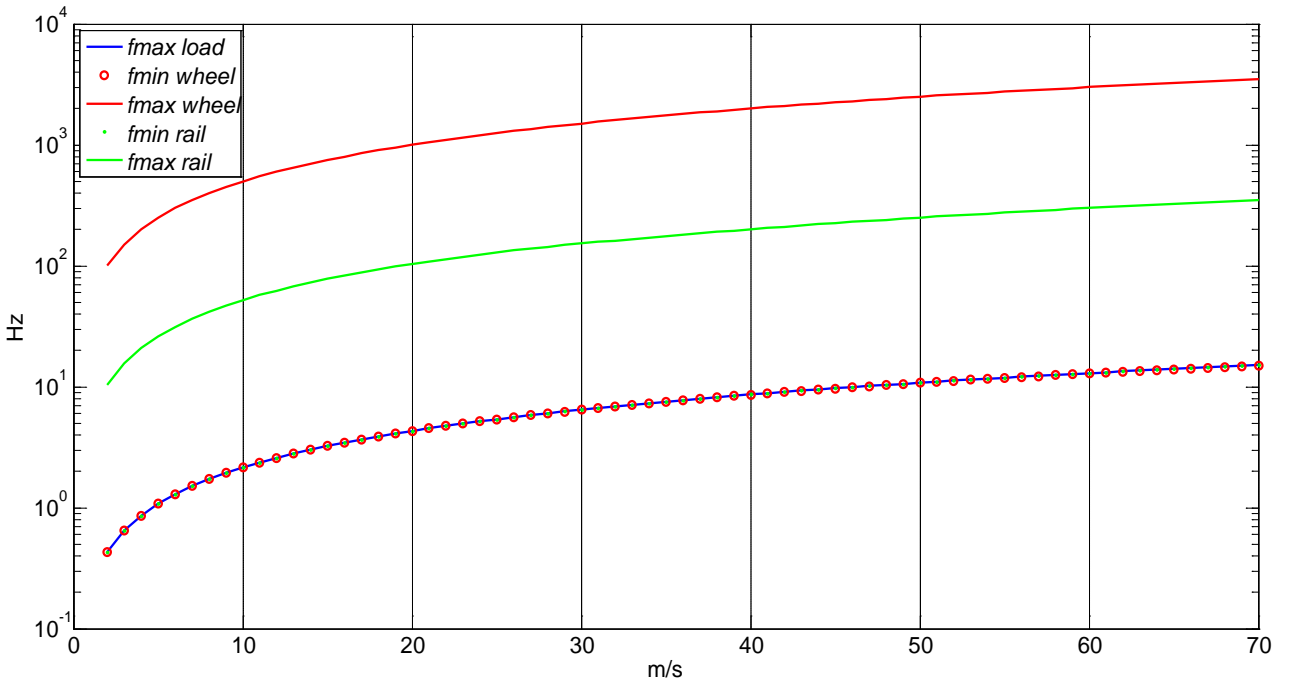


Figure 5: Frequency bandwidth related to the load effect, to the wheel and rail roughness plotted versus the train speed.

The previous results show the following characteristics of the spectra:

- (i) the train load spectrum develops in a low frequency range with respect to the others. However, a certain overlap is observed with the lowest frequency components of both the random-wheel and random-rail loads.
- (ii) The two random loads overlap even if a much wider frequency spectrum characterizes the random-wheel load.
- (iii) The faster the train the lower the overlap between train load and random loads.



One of the conclusion is that a simple frequency filtering of the data cannot separate the three contributions. This means that additional data treatment should be used suitably manipulating the data in both the time and the frequency domains, and using statistical properties of the random data. More precisely, the separation of the train load from the random load is operated by the following operations:

- a) high-pass filter in the frequency domain;
- b) data chopping in the time domain.

Once the random load contribution is separated, the splitting of the wheel and rail components is made indeed following the procedure ahead:

- (i) the matrix data set is built, organized by row and columns, associated respectively to wagons and measurement stations ;
- (ii) assuming stochastic independency of cross signals along this matrix, and between random-rail and random-wheel processes, an algorithm able to extract the desired information, i.e. the rms value of roughness of both the portions of rail close to each measurement station and of the wheels of each wagon, is produced.

This process is described in the following section.

LOAD	BANDWIDTH	V=10m/s	V=20m/s	V=50m/s
$mg \delta(x-Vt)$ Train load	$[0, k^{(mg)}V]$ $k$ from equation (1)	0-2.1 Hz	0-4.4 Hz	0-10.9 Hz
$m\ddot{r}(t)\delta(x-Vt)$ Random-wheel	$[k_{\min}^{(wheel)}V, \omega_{\max}^{(wheel)} + k_{\max}^{(wheel)}V]$ $k$ from equation (2)	2.1-503 Hz	3.9-1015 Hz	17-2561 Hz
$m\ddot{h}(t)\delta(x-Vt)$ Random-rail	$[k_{\min}^{(rail)}V, \omega_{\max}^{(rail)} + k_{\max}^{(rail)}V]$ $k$ from equation (2)	2.2-52 Hz	4.4-104 Hz	11-267 Hz

Table II: Spectra of different load components.

### 3.3 Wheel and rail roughness identification

Based on the previous analysis, the complete expression of the strain time history takes the form:

$$\varepsilon(x, t) = \frac{EI}{W_f^*} \frac{\partial^2}{\partial x^2} \left[ \sum_{n=1}^N C_n^{(rail)} \Phi_{ma_w}^{n(rail)}(x-Vt) e^{j \frac{2\pi n V}{L} t} + \sum_{n=1}^N C_n^{(wheel)} \Phi_{ma_w}^{n(wheel)}(x-Vt) e^{jn\Omega t} + \Phi_{mg}(x-Vt) \right]$$

This represents the strain response to a single travelling wheel. Considering a set of  $N_w$  wheel travelling together and mounted at distances  $l_h$  with respect to a given reference point, the expression must be modified as follows:

$$\varepsilon(x, t) = \frac{EI}{W_f^*} \sum_{h=1}^{N_w} \left[ \sum_{n=1}^N C_n^{(rail)} \Phi_{ma_w}^{n(rail)}(x-Vt-l_h) e^{j \frac{2\pi}{L} (Vt-l_h)} + \sum_{n=1}^N C_{nh}^{(wheel)} \Phi_{ma_w}^{n(wheel)}(x-Vt-l_h) e^{jn\Omega t} + \Phi_{mg}''(x-Vt-l_h) \right]$$

Using a more compact notation, we characterize the response at the measurement station  $k$  when the rail is loaded by the whole set of wheels:

$$\varepsilon(x_k, t) = \sum_{h=1}^{N_w} \eta_{hk}^{(rail)}(t) + \eta_{hk}^{(wheel)}(t) + \frac{EI}{W_f^*} \Phi_{mg}''(x_k - Vt - l_h)$$

The first step consists in applying a high-pass frequency filter with the cut-off frequency close to the maximum frequency of the train load (see table 1). This reduces the contribution of the third term in the previous equation that is modified as:



$$\varepsilon^F(x_k, t) = \sum_{h=1}^{N_w} \eta_{hk}^{(rail)}(t) + \eta_{hk}^{(wheel)}(t) + R_{hk}(t)$$

where the superscript  $F$  over the  $\eta$ 's is omitted, and

$$R_{hk} \ll \frac{EI}{W_f^*} \Phi_{mg}''(x_k - Vt - l_h)$$

The residual term  $R_{hk}$  is still present but its contribution is sharply localized in the time domain, at the instants where the wheels are in correspondence of the sensor location. These small peaks can be eliminated by chopping those small signal intervals from the data.

$$\varepsilon^{FC}(x_k, t) = \left[ \sum_{h=1}^{N_w} \eta_{hk}^{(rail)}(t) + \eta_{hk}^{(wheel)}(t) \right]$$

The final splitting of the two random components is operated by considering the correlation matrix  $\mathbf{C}$  built by the signals  $\varepsilon^{FC}(x_k, t)$ , or the power spectral density matrix  $\mathbf{S}$ :

$$C_{ij}(\tau) = \langle \varepsilon^{FC}(x_i, t) \varepsilon^{FC}(x_j, t + \tau) \rangle, \quad S_{ij}(\omega) = FT\{C_{ij}(\tau)\}$$

where  $FT$  is the Fourier transform. Thus:

$$C_{ij}(\tau) = \left\langle \left[ \sum_{h=1}^{N_w} \eta_{hi}^{(rail)}(t) + \eta_{hi}^{(wheel)}(t) \right] \left[ \sum_{k=1}^{N_w} \eta_{kj}^{(rail)}(t + \tau) + \eta_{kj}^{(wheel)}(t + \tau) \right] \right\rangle$$

We assume: (i) the wheel-rail, wheel-wheel for different pair of wheels, and rail-rail for different measurement stations, are statistically independent random processes. Formally:

$$Hp \text{ (i)} \rightarrow \left\langle \sum_{h,k=1}^{N_w} \eta_{hi}^{(wheel)}(t) \eta_{ki}^{(rail)}(t + \tau) \right\rangle = \left\langle \sum_{h,k=1}^{N_w} \eta_{hi}^{(rail)}(t) \eta_{ki}^{(wheel)}(t + \tau) \right\rangle = 0$$

$$Hp \text{ (ii)} \rightarrow \left\langle \sum_{h,k=1}^{N_w} \eta_{hi}^{(wheel)}(t) \eta_{kj}^{(wheel)}(t + \tau) \right\rangle = \left\langle \sum_{h=1}^{N_w} \eta_{hi}^{(wheel)}(t) \eta_{hj}^{(wheel)}(t + \tau) \right\rangle \delta_{ij}$$

$$Hp \text{ (iii)} \rightarrow \left\langle \sum_{h,k=1}^{N_w} \eta_{hi}^{(rail)}(t) \eta_{kj}^{(rail)}(t + \tau) \right\rangle = \left\langle \sum_{h=1}^{N_w} \eta_{hi}^{(rail)}(t) \eta_{hj}^{(rail)}(t + \tau) \right\rangle \delta_{ij}$$

Thus, the auto-correlation matrix is diagonal and its non-zero terms are:

$$C_{ii}(\tau) = \sum_{h=1}^{N_w} \langle \eta_{hi}^{(rail)}(t) \eta_{hi}^{(rail)}(t + \tau) \rangle + \sum_{h=1}^{N_w} \langle \eta_{hi}^{(wheel)}(t) \eta_{hi}^{(wheel)}(t + \tau) \rangle$$

For  $\tau = 0$  the diagonal terms are:

$$C_{ii}(0) = \sum_{h=1}^{N_w} \langle \eta_{hi}^{(rail)2}(t) \rangle + \sum_{h=1}^{N_w} \langle \eta_{hi}^{(wheel)2}(t) \rangle$$

This can be considered the statistical characterization of the strain response produced by a single car of the train, typically having  $N_w=4$  wheels. Identifying by  $c$  the signal associated to the  $c$ -th car, produces the set of  $N_C$  signals:

$$\varepsilon_c^{FC}(x_k, t) = \sum_{h=1}^{N_w} \left[ \eta_{hkc}^{(rail)}(t) + \eta_{hkc}^{(wheel)}(t) \right]$$

to which the described procedure associates the auto-correlation coefficients:

$$C_{ii}^c(0) = \left\langle \varepsilon_c^{FC^2}(x_i, t) \right\rangle = \sum_{h=1}^{N_w} \left\langle \eta_{hkc}^{(rail)^2}(t) \right\rangle + \sum_{h=1}^{N_w} \left\langle \eta_{hkc}^{(wheel)^2}(t) \right\rangle = E_{ci}^{(rail)^2} + E_{ci}^{(wheel)^2}$$

The correlation coefficients  $C_{ij}$  contain the information about wheel and rail irregularities. Note that  $E_{ci}^{(rail)^2}$ ,  $E_{ci}^{(wheel)^2}$  represent the strain response as a superposition of two independent effects: the first is the response of perfectly circular wheels rolling on a rough rail, the second is the response of a flat rail when irregular wheels roll on it. For this reason we assume that  $E_{ci}^{(rail)^2} = E_i^{(rail)^2}$  is independent of the car index  $c$ . Analogously we assume that  $E_{ci}^{(wheel)^2} = E_c^{(wheel)^2}$  is independent of the station index  $i$ . With these last simplifications, we are in the position to identify  $E_i^{(rail)^2}$  and  $E_c^{(wheel)^2}$  that is a set of  $N_S+N_C$  unknowns. Considering the following summations, and using the previous simplifications, one has:

$$\begin{aligned} \sum_{c=1}^{N_c} \left\langle \varepsilon_c^{FC^2}(x_i, t) \right\rangle &= \sum_{c=1}^{N_c} \left[ E_{ci}^{(rail)^2} + E_{ci}^{(wheel)^2} \right] \approx N_C E_i^{(rail)^2} + \sum_{c=1}^{N_c} E_c^{(wheel)^2} \\ \sum_{i=1}^{N_s} \left\langle \varepsilon_c^{FC^2}(x_i, t) \right\rangle &= \sum_{i=1}^{N_s} \left[ E_{ci}^{(rail)^2} + E_{ci}^{(wheel)^2} \right] \approx N_S E_c^{(wheel)^2} + \sum_{i=1}^{N_s} E_i^{(rail)^2} \end{aligned}$$

that produce the system of  $N_S+N_C$  algebraic equations in terms of the introduced unknowns:

$$\begin{aligned} E_i^{(rail)^2} + \frac{1}{N_C} \sum_{c=1}^{N_c} E_c^{(wheel)^2} &= \frac{1}{N_C} \sum_{c=1}^{N_c} \left\langle \varepsilon_c^{FC^2}(x_i, t) \right\rangle \\ \frac{1}{N_S} \sum_{i=1}^{N_s} E_i^{(rail)^2} + E_c^{(wheel)^2} &= \frac{1}{N_S} \sum_{i=1}^{N_s} \left\langle \varepsilon_c^{FC^2}(x_i, t) \right\rangle \end{aligned} \tag{3}$$

where the rhs terms are known from the optical strain measurements along the rail. Eq. (3) in matrix notations reads:

$$\mathbf{Bz} = \mathbf{E}$$

where:

$$\mathbf{B} = \begin{bmatrix} 1 & 0 & \cdots & 0 & 1/N_C & 1/N_C & \cdots & 1/N_C \\ & & \ddots & & & & & \\ & & & & & & & \\ 0 & \cdots & 0 & 1 & 1/N_C & \cdots & & 1/N_C \\ 1/N_S & \cdots & & 1/N_S & 1 & 0 & \cdots & 0 \\ & & & & & \ddots & & \\ & & & & & & & 0 \\ 1/N_S & & & 1/N_S & 0 & \cdots & 0 & 1 \end{bmatrix}$$

$$\mathbf{z} = \begin{Bmatrix} E_1^{(rail)^2} \\ \vdots \\ E_{N_S}^{(rail)^2} \\ E_1^{(wheel)^2} \\ \vdots \\ E_{N_C}^{(wheel)^2} \end{Bmatrix}, \quad \mathbf{E} = \begin{Bmatrix} \frac{1}{N_C} \sum_{c=1}^{N_C} \langle \varepsilon_c^{FC2}(x_1, t) \rangle \\ \vdots \\ \frac{1}{N_C} \sum_{c=1}^{N_C} \langle \varepsilon_c^{FC2}(x_{N_S}, t) \rangle \\ \frac{1}{N_S} \sum_{i=1}^{N_S} \langle \varepsilon_1^{FC2}(x_i, t) \rangle^2 \\ \vdots \\ \frac{1}{N_S} \sum_{i=1}^{N_S} \langle \varepsilon_{N_C}^{FC2}(x_i, t) \rangle^2 \end{Bmatrix}$$

Unfortunately, the block matrix  $\mathbf{B}$  is singular and its rank is  $N_C+N_S-1$ , which means one equation of the system (3) is a linear combination of the others. The problem is eschewed imposing the additional condition:

$$\frac{1}{N_S} \sum_{i=1}^{N_S} E_i^{(rail)^2} = \frac{cost}{N_C} \sum_{c=1}^{N_C} E_c^{(wheel)^2} \rightarrow \mathbf{B} = \begin{bmatrix} 1 & 0 & 0 \\ & \ddots & \\ 0 & 0 & 1 \end{bmatrix} + \begin{bmatrix} 0 & \cdots & 0 & 1/N_C & 1/N_C \\ \vdots & & & \vdots & \vdots \\ & & & \vdots & cost/N_C & cost/N_C \\ 0 & \cdots & 0 & \vdots & \vdots \end{bmatrix} \quad (4)$$

where the constant  $cost$  is estimated from the experimental data. The solution of eq. (3) is then:

$$\mathbf{z} = \mathbf{B}^{-1} \mathbf{E} \quad (5)$$

The physical basis of eq. (4) is the following. The form on the rhs represents an index of the average irregularity of the whole rail along the monitored track, that, apart severe special damage events, can be considered aligned with the wear data of the rail, mainly depending of the track aging. The form on the lhs s indeed a measure of the average irregularity of the set of the train wheels. In addition, in this case we can assume again, apart special damage events, the wear is aligned with the data depending on the train aging.

With these assumptions, the two terms compared by eq. (4) have the role of “universal” constants associated with the expected average wears for given ages of rail track and trains, where constants means these parameters are very slowly varying in the time windows where the data are required.

The hypothesis made on the constancy of  $\frac{1}{N_C} \sum_{c=1}^{N_C} E_c^{(wheel)^2}$  has been verified considering the acquired data:

this quantity does not depend significantly on different train passages. The hypothesis made on the constancy

of  $\frac{1}{N_s} \sum_{i=1}^{N_s} E_i^{(rail)^2}$  is indeed substantially self-evident one expects very slow drift of it, depending on the track age.

## 4 Results and discussion

The typical strain time history acquired by a FBG sensor, when a six-car passenger train crosses a measurement station is shown in Fig. 6. The passage of the 24 axles are clearly indicated by the peaks in the signal, the highest strain peak is roughly  $55 \mu\epsilon$ : given the axle spacing, the evaluation of the train speed is straightforward. The deformation of the rail depends on the train speed and weight as well as on the maintenance conditions of rail and wheels. As explained in the previous section, the low frequency, highly energetic, peaks are due to the train load, while the signal enclosed between the peaks is characterised by higher frequencies, produced by irregularities of the wheel-rail contact.

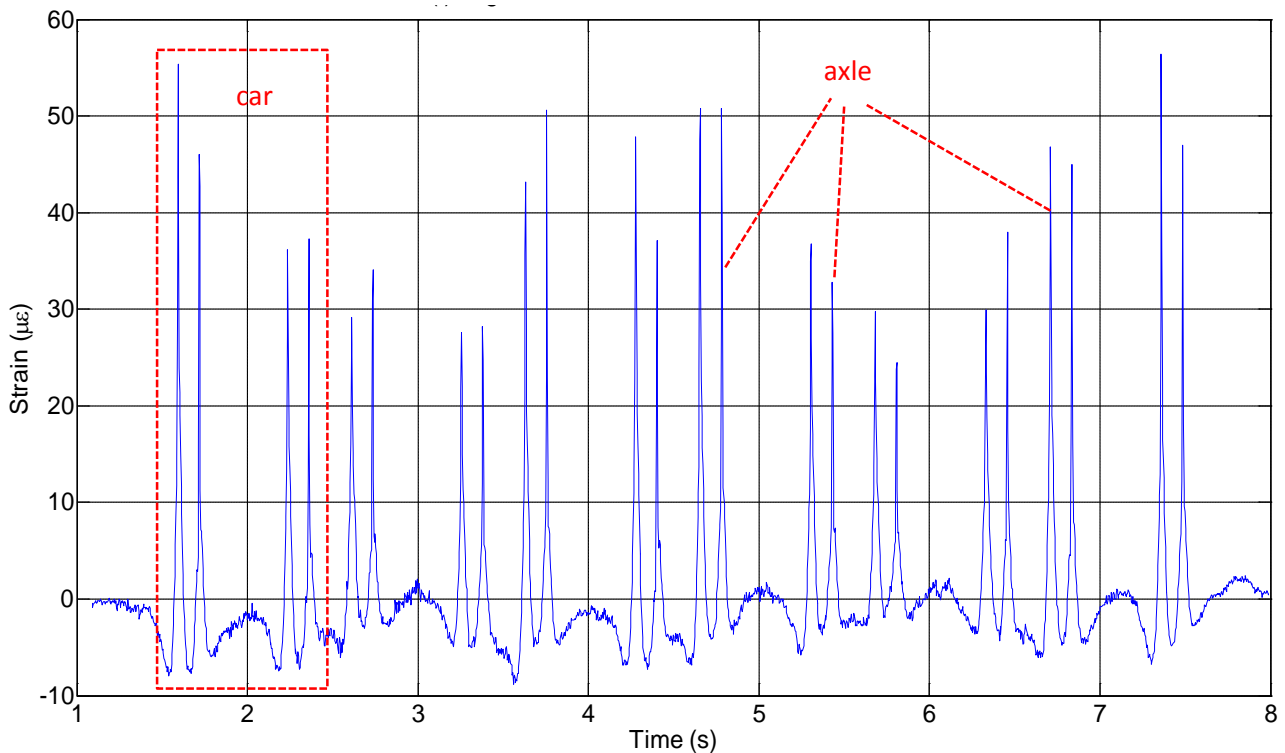


Figure 6: Strain signal recorded by a FBG sensor, induced by a six-car passenger train.

Fig. 7 shows the zooms of Fig. 6, related to the recorded strain induced by the passage of each car, while Fig. 8 shows the low-pass filter of the strain signal, employing a filter with a cut-off frequency of 20 Hz is applied to the recorded strain: the low pass signal mainly contains the information relative to the train weight.

Fig. 9 shows the Fourier transform of the strain signal. Most of the energy is stored around 10 Hz, which is the frequency related to the rolling wheels:  $f_{load} = v/(2\pi R) \approx 7Hz$ , with  $v \approx 17m/s$ ,  $R = 0.4m$ . The presence of a peak around  $f_{load}$  may show a flat spot in one, or more wheels, of a car, which is a visible abrasion in the outer surface of the wheel and dissipates a large amount of energy during the periodical impact of the plane zone of the wheel with the rail. In Fig. 9 there is no evident peak around  $f_{load}$  in any car of the train.

In order to obtain an index concerning the condition of the wheels and of the rail, the signal is normalised with the mean value of the peaks, which depends on the train load, and with the train velocity. The first subplot in Fig. 10 shows the normalized high-pass filter of the strain signal, the sharp peaks point out the influence of the axles load has not been completely removed from the filter. The second subplot in Fig. 10 shows the portions of the high-frequency signal obtained chopping the data from a single boogie form the signal (the data within two consecutive peaks of different boogies): these zones are mildly affected by the train load.

Using the high-frequency, chopped, signals, shown in the second subplot in Fig. 10,  $\varepsilon_{c,k}^{FC}(t)$ , where subscripts  $c$  and  $k$  are for the car and the FBG station, respectively, the power of the signal is computed:

$$\langle \varepsilon_c^{FC2}(x_i, t) \rangle = \frac{1}{n} \sum_{j=1}^n \left( \varepsilon_c^{FC2}(x_i, t_j) \right)^2$$

where  $n$  is the number of time steps of the signal for the  $c$ -th car. The index related to wheels and rail condition are readily obtained from eq. (5), considering 21 FBG-stations and setting  $cost=1$  from experimental trials.

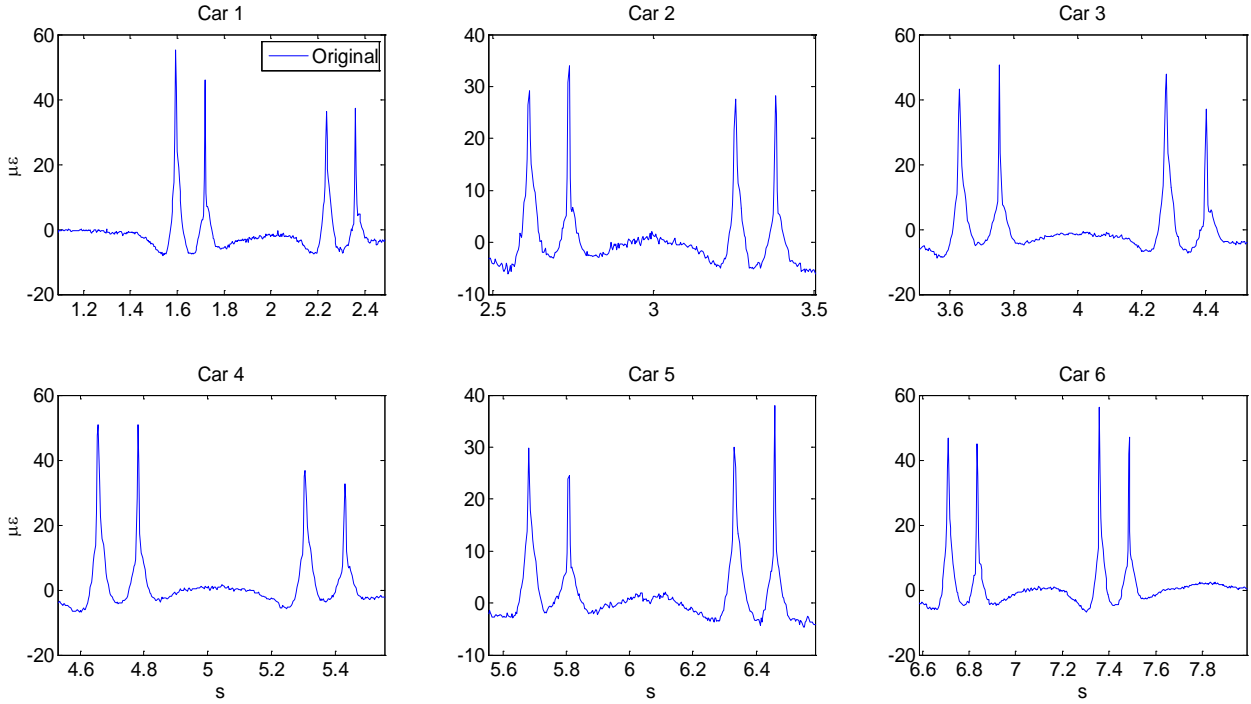


Figure 7: Each subplot shows the strain in Fig. 6 induced by each car of the train.

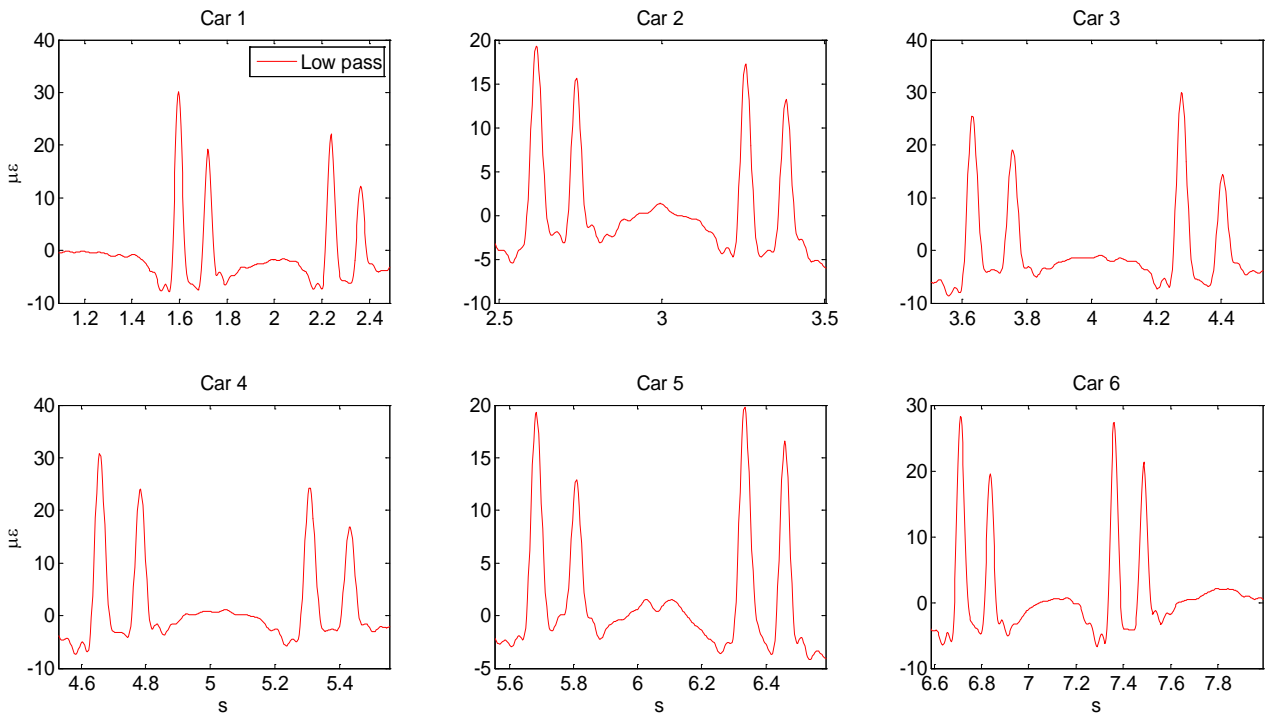


Figure 8: Low-pass filter of the strain signals in Fig. 7.

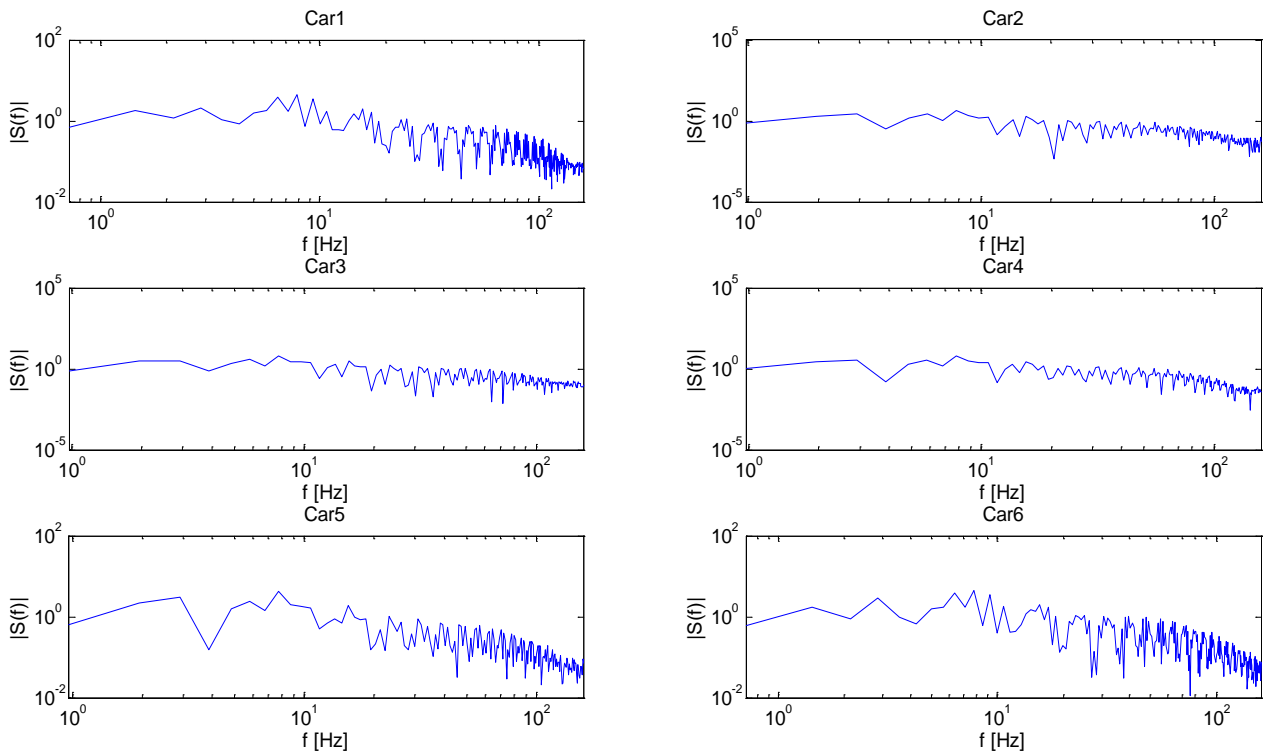


Figure 9: FFT of the signal in Fig. 7.

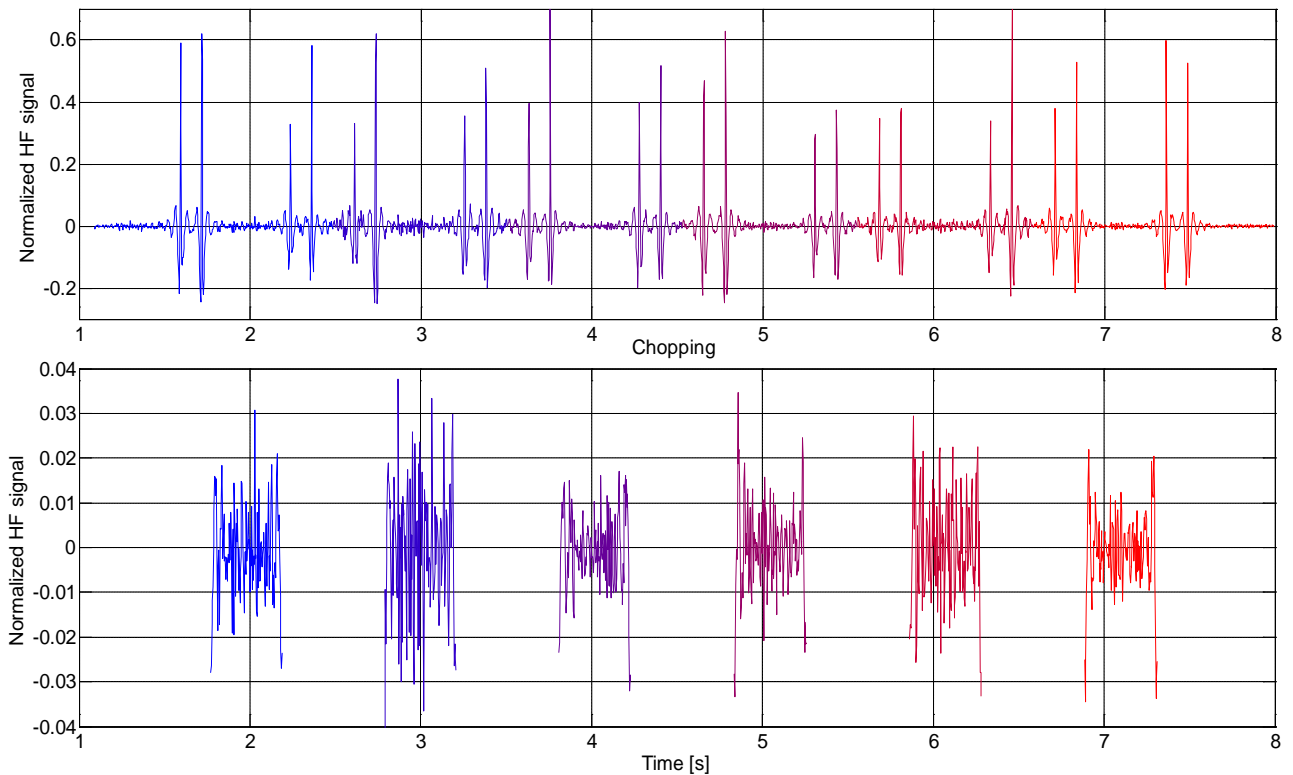


Figure 10: Starting from the subplot on top, normalized high-pass filter of the strain signal of Fig. 6, and the corresponding chopped parts of the signal.

Using the compact notation:

$$R_i = E_i^{(rail)^2}, W_c = E_c^{(wheel)^2}$$

and using eq. (5), Fig. 11 shows the rail index  $R_i$  for 110 different train passages, considerations follow ahead:

- the rail around the 19<sup>th</sup> FBG station is in the worst condition, since it has the highest index, far greater than the others. Fig. 13 shows the corresponding strain acquisition for the 44<sup>th</sup> train passage, the *noise* between the peaks is relevant and is the result of deep irregularities around the station;
- the rail segments around the 5<sup>th</sup>, 9<sup>th</sup> and 3<sup>th</sup> FBG stations are in the best conditions, since the rail indexes have here the smallest values. Negative values of the index have no physical meaning, as eq. (3) shows, and should be disregarded. This is a limit of the present technique, coming from the hypothesis *HP i*), *ii*) and *iii*) made in the previous section, which, sometimes, arises when the working conditions of the rail around the FBG station are very good. Fig. 7 shows the strain acquisition related to the 5<sup>th</sup> FBG station at the 40<sup>th</sup> train passage, the modest *noise* between the peaks confirms the low level of irregularities around the station;
- the regions of the rail around the 16<sup>th</sup>, 1<sup>st</sup>, 2<sup>nd</sup> and 3<sup>rd</sup> are also in pretty bad conditions;
- the variability shown by the different bars along the same FBG station is mainly due to the interaction of different wheels with the same part of the rail, which is not a completely independent random process;
- there are three outliers in the data, i.e. three values very far from the others, located at the 4<sup>th</sup>, the 18<sup>th</sup> and the 21<sup>th</sup> FBG stations. These values are due to errors occurred during the acquisition of the strain signal, as it is shown in Fig. 14, and should be disregarded.

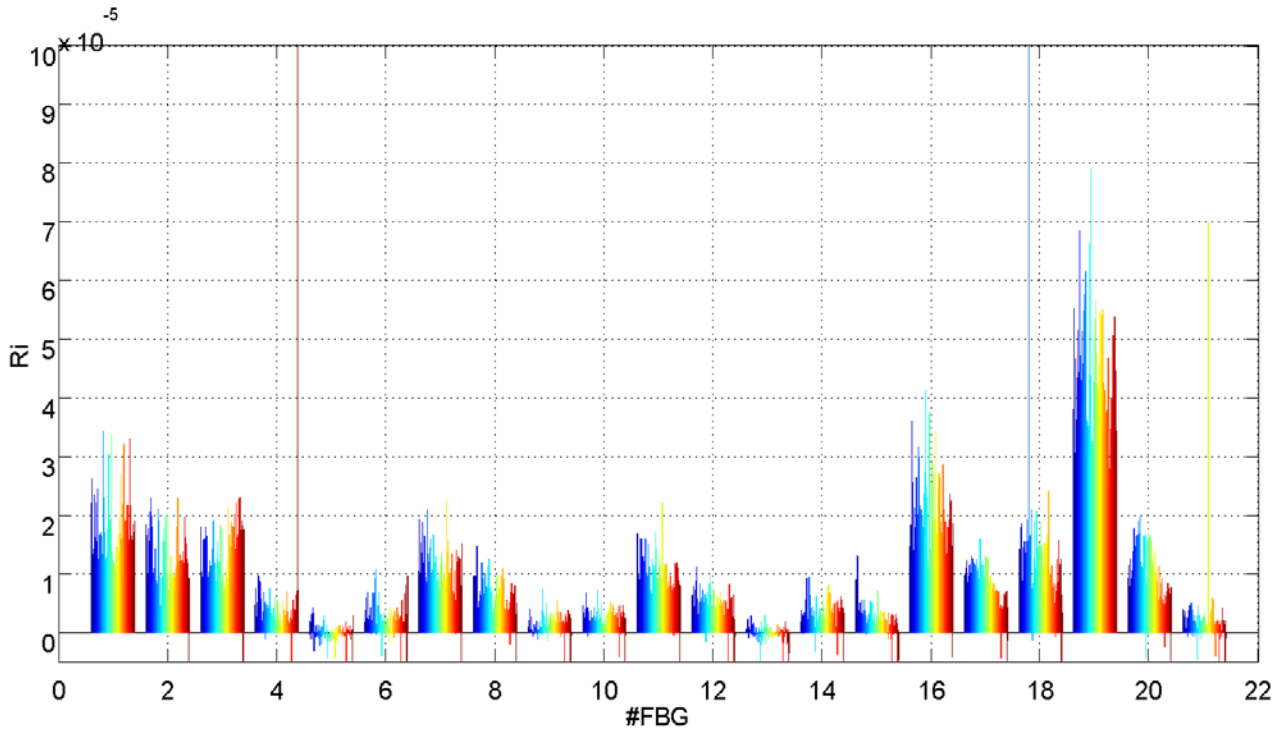


Figure 11: Bar graph of  $R_i$  for 110 train passages plotted versus the 21 FBG stations. The bar colours identifies different passages, as in Fig. 12.

Related considerations are made for Fig. 15, which shows the wheel index  $W_c$  :

- bars of the same colour provide information regarding the status of the wheels of the cars for the same train. It was not possible normalising the indexes with a proper scaling factor, because we did not have any information about the identity of the running trains and when the wheels were reprofiled.
- The average damage is higher for the wheels of the 2<sup>nd</sup> and the 5<sup>th</sup> cars, roughly double than the other. It is interesting to correlate this information with the average car load shown in Fig. 16, which shows the 2<sup>nd</sup> and the 5<sup>th</sup> cars have the smallest load, in fact they are the only cars that do not mount electric motors. This, rather counterintuitive, result may arise from two effects:
  - vibrations induced by the wheel - rail contact are probably higher in light cars, that have an higher resonant frequency of the suspensions, somehow tuned with the typical wavelength of the wheel irregularities;



- due to higher vibrations and lighter car load, the wheels may frequently lose the contact with the rail track, giving rise to shocks along the contact patch.

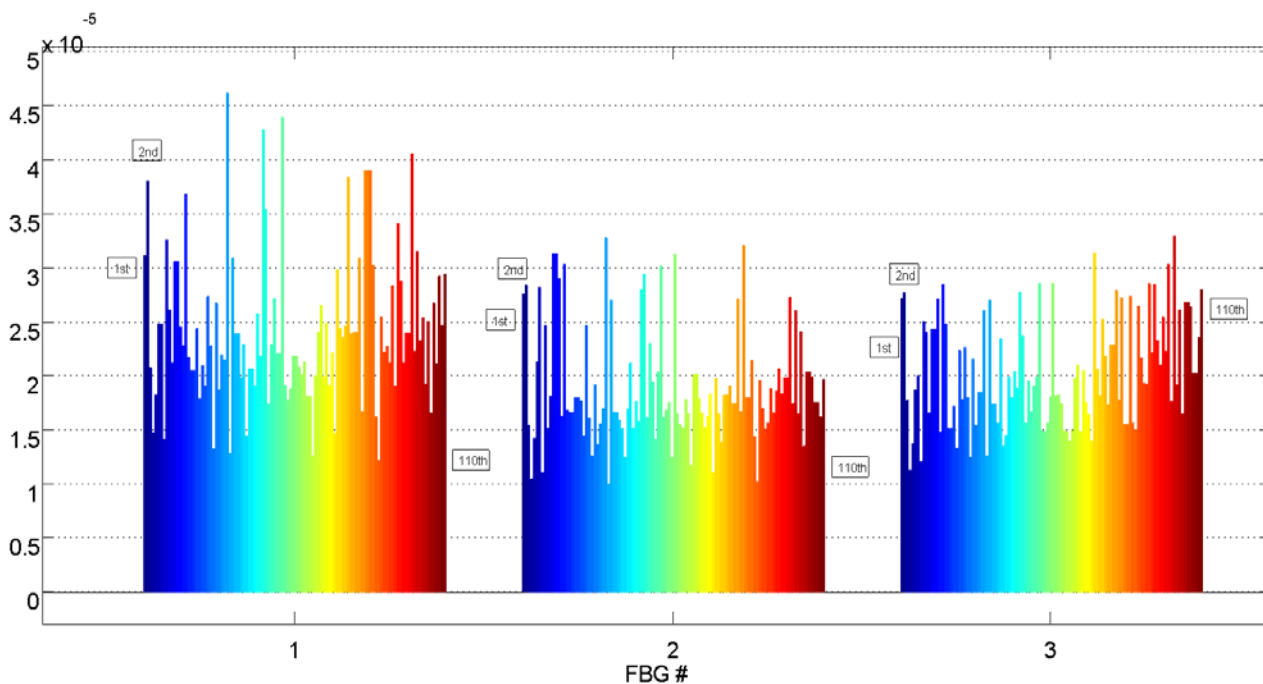


Figure 12: Magnification of fig 11, where all the 110 different bars corresponding to different passages, are clearly visible.

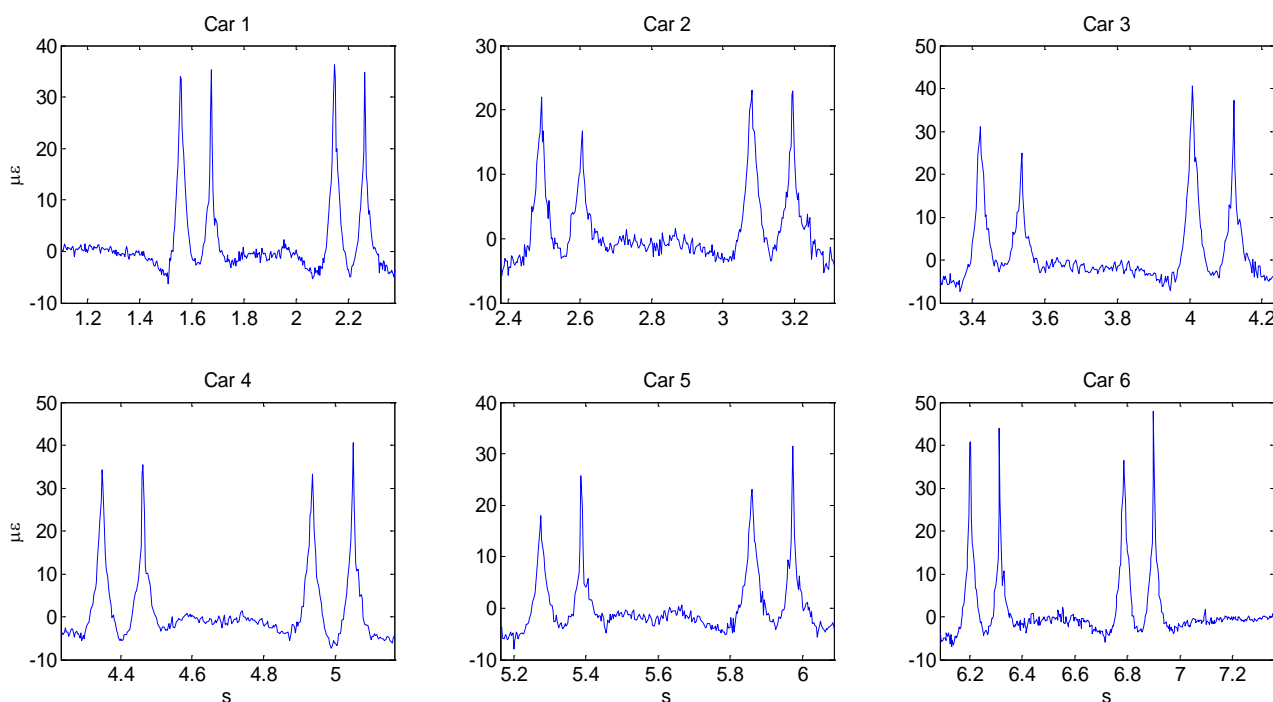


Figure 13: Time history of the strain acquired at the 19<sup>th</sup> FBG station for the 44<sup>th</sup> train passage.

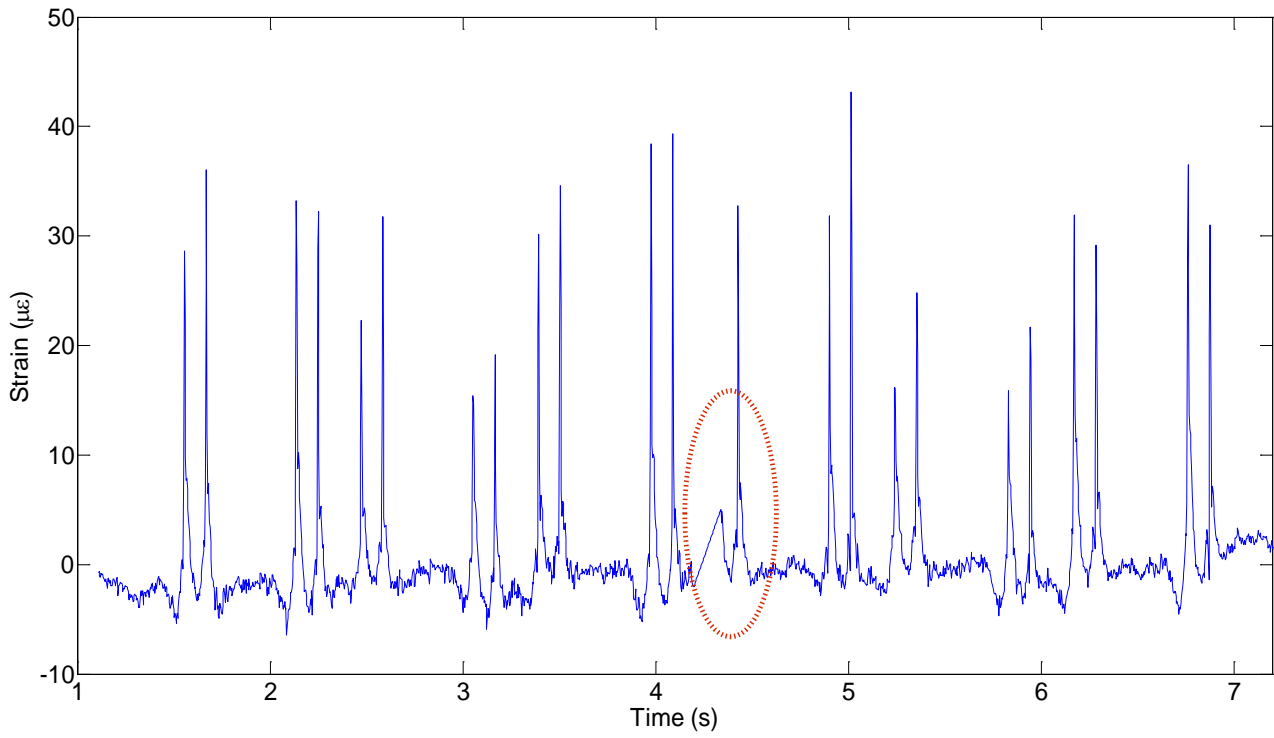


Figure 14: Data acquisition error, in the dashed circle, which harms the identification algorithm with outlier.

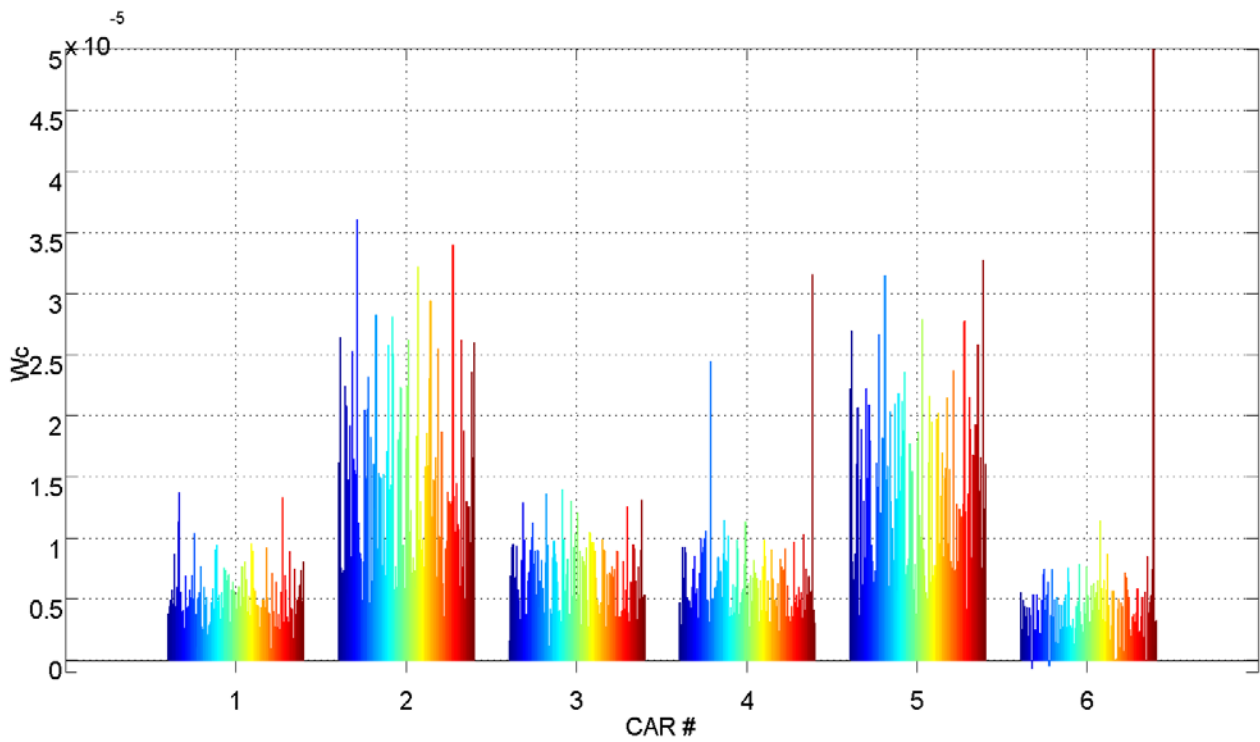


Figure 15: Bar graph of  $W_c$  for 110 train passages plotted versus the cars.

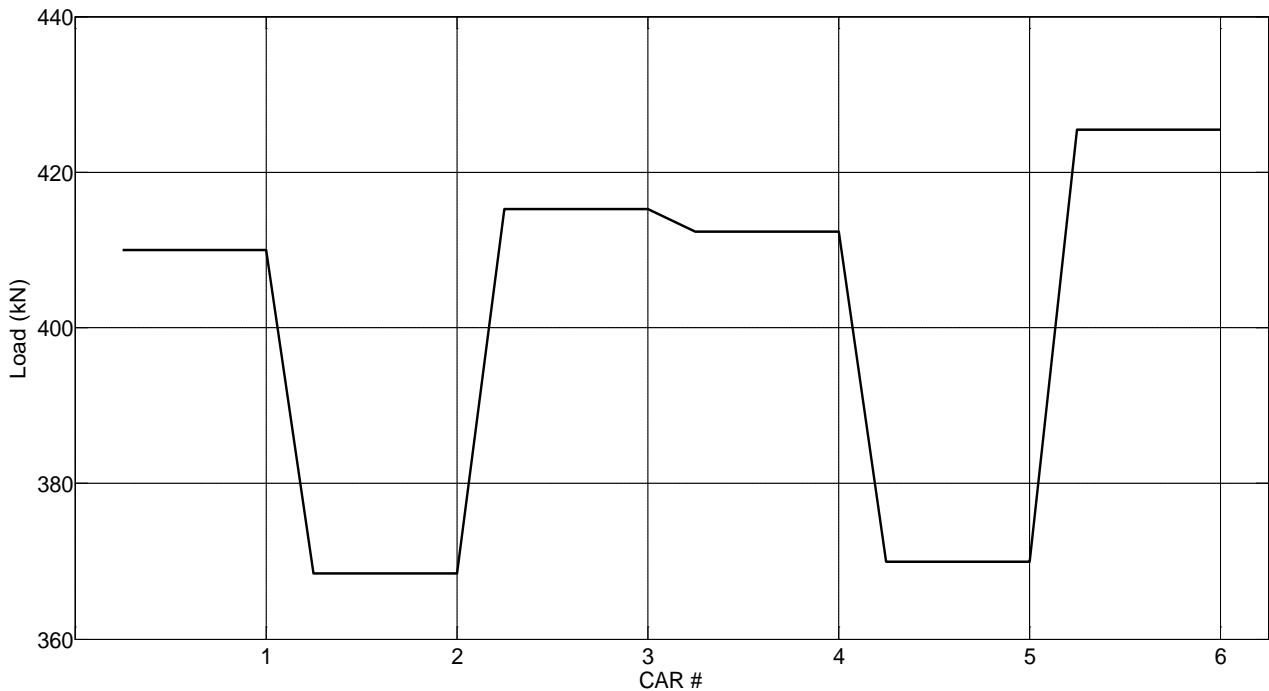


Figure 16: Average axle load extrapolated from the strain acquisition for 110 train passages.

## 5 Concluding remarks

The paper presents a novel technique for the data acquisition and post-processing, coming from distributed FBG sensors along a railway track. Aim of the system is the monitoring and identification of both the rail as well as the train wheels roughness, as indicators of their health status.

The theoretical background shows the separation of the information coming from wheels and rail track is conceptually difficult. In fact, it emerges a partial frequency overlap of the related signal components that does not permit the simple separation by filters. The processing technique is therefore more sophisticated and uses both frequency filters, time domain chopping and time and ensemble averages, to extract individual information on roughness of each train car and along the track.

The perspectives of this monitoring technique are very interesting, allowing real-time simultaneous scanning and monitoring of the rail and wheels, which are key tasks for the railways maintenance service. Future developments rely on tests for the creation of benchmarking signals that will allow the identification of threshold levels for the identified roughness, representing real alerts for the maintenance service to inspect the train and/or rail.

Now the extracted data provide the railways management with information of the relative degree of damage along the rail track, identifying locations responsible for the highest roughness due to wear, and the identification of the cars with the worst wheels conditions. The systems is able to identify roughness properties of distributed random damages, but in a next future a new algorithm, based on Hilbert-Huang transformation [12, 13] will be available and capable of extracting information on deterministic localised spot-like damages.

## Acknowledgments

The experimental set-up was installed by GCF [14] and Acesystem [15], companies operating in the field of maintenance services and measurement sensors. The analysis presented in this paper has been carried out on data made available by Acesystem, in the context of a common research project together with Sapienza university of Rome.

## References

- [1] Salawu, O. S., Detection of structural damage through changes in frequency: a review, *Eng. Struct.* 1997; 19, 9, 718–723.
- [2] Doebling, S. W., Farrar, C. R., Prime, M. B., A summary review of vibration-based damage identification methods, *Shock Vib. Dig.* 1998; 30, 2, 91–105.
- [3] A. D. Kersey, M. A. Davis, H. J. Patrick, M. LeBlanc, K. P. Koo, C. G. Askins, M. A. Putnam, and E. J. Friebele, “Fiber grating sensors,” *J. Lightw. Technol.*, vol. 15, no. 8, pp. 1442–1463, Aug. 1997.
- [4] M. Guagliano and M. Pau, “An experimental-numerical approach for the analysis of internally cracked railway wheels,” *Wear*, vol. 265, no. 9-10, pp. 1387–1395, 2008.
- [5] E. Matzan, “System for detection of defects in railroad car wheels,” U.S. Patent 7213789, 2007.
- [6] K. Kincade, “Fibre sensors lay groundwork for structural health monitoring,” *Laser Focus World*, vol. 42, no. 2, pp. 63–67, 2005.
- [7] F. Ansari, Ed. Dordrecht, *Sensing Issues in Civil Structural Health Monitoring*, Holland: Springer, 2005.
- [8] Chu-liang Wei, Chun-cheung Lai, Shun-ye Liu, W. H. Chung, T. K. Ho, Hwa-yaw Tam, S. L. Ho, A. McCusker, J. Kam, and K. Y. Lee, A Fiber Bragg Grating Sensor System for Train Axle Counting, *IEEE sensors journal*, vol. 10, no. 12, pp 1905-1912, 2010.
- [9] B. Glisic and D. Inaudi, *Fibre Optic Methods for Structural Health Monitoring*. New York: Wiley, 2007
- [10] A. López-Pita, *Infraestructuras Ferroviarias*. Barcelona, Spain: Ediciones UPC, 2006.
- [11] C. Barbosa, N. Costa, L. A. Ferreira, F. M. Araujo, H. Varum, A. Costa, C. Fernandes, and H. Rodrigues, “Weldable fibre Bragg grating sensors for steel bridge monitoring,” *Meas. Sci. Technol.*, vol. 19, p. 125305, 2008.
- [12] N. Roveri, A. Carcaterra, “Damage detection in structures under travelling loads by Hilbert–Huang transform”, *Mechanical Systems and Signal Processing*, (2011), doi:10.1016/j.ymssp.2011.06.018.
- [13] N. Roveri, A. Carcaterra, “Unsupervised identification of damage and load characteristics in time-varying systems” *Mathematical Models of Continuous Mechanics*, (2013), submitted.
- [14] <http://www.gcf.it/>
- [15] <http://www.acesys.it/>